Seasonal variation of nitryl chloride and its relation to gas-phase precursors during the JULIAC campaign in Germany

Zhaofeng Tan[1], Hendrik Fuchs[1,4], Andreas Hofzumahaus[1], William J. Bloss[3], Birger Bohn[1], Changmin Cho[1], Thorsten Hohaus[1], Frank Holland[1], Chandrakiran Lakshmisha[1], Lu Liu[1], Paul S. Monks[2], Anna Novelli[1], Doreen Niether[1], Franz Rohrer[1], Ralf Tillmann[1], Thalassa Valkenburg[2], Vaishali Vardhan[1,a], Astrid Kiendler-Scharr[1,4], Andreas Wahner[1], Roberto Sommariva[2,3]

[1] Institute of Energy and Climate Research, IEK-8: Troposphere, Forschungszentrum Jülich GmbH, Jülich, Germany

[2] School of Chemistry, University of Leicester, Leicester, UK

[3] School of Geography, Earth and Environmental Sciences, University of Birmingham, Birmingham, UK

[4] Physikalisches Institut, Universität zu Köln, Köln, Germany

[a] now at, Department of Chemistry, University College Cork, Ireland

Correspondence: Zhaofeng Tan (zh.tan@fz-juelich.de) and Roberto Sommariva (rs445@le.ac.uk)

Abstract. Ambient measurements of nitryl chloride ($ClNO_2$) were performed at a rural site in Germany covering 3 periods in winter, summer, and autumn 2019 as part of the JULIAC campaign (Jülich Atmospheric Chemistry Project) that aimed for understanding the photochemical processes in air masses typical for mid-west Europe. Measurements were conducted at 50 m above ground, which was mainly located in the nocturnal boundary layer and thus uncoupled from local surface emissions. $ClNO_2$ is produced at nighttime by heterogeneous reaction of dinitrogen pentoxide (N_2O_5) on chloride (Cl^-) containing aerosol. Its photolysis during the day is of general interest as it produces chlorine (Cl) atoms that react with different atmospheric trace gases forming radicals. The highest observed $ClNO_2$ mixing ratio was 1.6 ppbv (15-min average) during the night of September 20. Air masses reaching the measurement site either originated from long-range transport from the southwest and had an oceanic influence or circulated in the nearby region and were influenced by anthropogenic activities. Nocturnal maximum $ClNO_2$ mixing ratios were around 0.2 ppbv if originating from long-range transport in nearly all seasons, while values were higher ranging from 0.4 to 0.6 ppbv for regionally influenced air. The chemical composition of long-range transported air was similar in all investigated seasons, while the

regional air exhibited larger differences between the seasons. The N_2O_5 necessary for $ClNO_2$ formation comes from the reaction of nitrate radicals (NO_3) with nitrogen dioxide (NO_2), where NO_3 itself is formed by reaction of NO_2 with ozone (O_3). Measured concentrations of $ClNO_2$, NO_2 and O_3 were used to quantify $ClNO_2$ production efficiencies, i.e., the yield of $ClNO_2$ formation per NO_3 radical formed, and a box model was used to examine the idealized dependence of $ClNO_2$ on the observed nocturnal O_3 and NO_2 concentrations. Results indicate that $ClNO_2$ production efficiency was most sensitive to the availability of NO_2 rather than that of O_3 and increase with decreasing temperature. The average $ClNO_2$ production efficiency was highest in February and September with values of 18% and was lowest in December with values of 3%. The average $ClNO_2$ production efficiencies were in the range of 3 and 6 % from August to November for air masses originating from long-range transportation. These numbers are at the high end of values reported in literature indicating the importance of $ClNO_2$ chemistry in rural environments in mid-west Europe.

1 Introduction

Nitryl chloride ($ClNO_2$) is an important nocturnal reservoir for nitrogen oxides (Brown and Stutz, 2012), because it accumulates during the night and photolyzes to nitrogen dioxide (NO_2) and a chlorine atom (Cl) after sunrise in the morning (Reaction R1).

$$ClNO_2 + h\nu \rightarrow NO_2 + Cl \quad \text{(R1)}$$

Chlorine atoms are a highly reactive oxidant in the atmosphere, initiating, for example, the degradation of volatile organic compounds (VOCs) and thereby contributing to the formation of ozone (O_3) and other pollutants (Simpson et al., 2015;Thornton et al., 2010;Mielke et al., 2011;Young et al., 2012). In some studies, $ClNO_2$ was shown to increase the daily ozone production from sub ppbv levels to mixing ratios of up to 10 ppbv, so that $ClNO_2$ chemistry contributed substantially to photochemical ozone production (Osthoff et al., 2008;Wang et al., 2016;Sommariva et al., 2021).

$ClNO_2$ formation is initiated by the heterogeneous reaction of dinitrogen pentoxide (N_2O_5) on aqueous surfaces that contains chloride (Cl^-) (Roberts et al., 2009;George and Abbatt, 2010;Osthoff et al., 2008;Thornton et al., 2010). The entire chemical reaction chain is described as McDuffie et al. (2018a):

$$NO_2 + O_3 \rightarrow NO_3 + O_2 \quad \text{(R2)}$$

$$NO_3 + NO_2 \rightarrow N_2O_5 \quad \text{(R3a)}$$

$$N_2O_5 \rightarrow NO_3 + NO_2 \quad \text{(R3b)}$$

$$N_2O_{5\,(g)} + \text{aerosol}_{(aq,Cl^-)} \rightarrow \varphi \times \left(ClNO_{2\,(g)} + HNO_{3\,(aq)}\right) + (1-\varphi) \times 2\,HNO_{3\,(aq)} \quad \text{(R4)}$$

where φ is the yield ($0 \leq \varphi \leq 1$) of gaseous $ClNO_2$ when N_2O_5 is taken up by aerosol.

$$NO_3 + VOCs \rightarrow \text{prod.} \quad \text{(R5)}$$

At night, nitrate radicals (NO_3) are produced by reaction of NO_2 with O_3 (Reaction R2), which then react with another NO_2 to form N_2O_5 (Reaction R3a). N_2O_5 decomposes thermally back to NO_2 and NO_3 (Reaction R3b). The forward and back reactions constitute a fast thermal equilibrium between NO_3 and N_2O_5 that is established quickly established at temperatures typically found in the lower troposphere (Brown and Stutz, 2012). Uptake of N_2O_5 on aqueous aerosol produces $ClNO_2$, when the particulate phase of the aerosol contains dissolved chloride. The yield (φ) of $ClNO_2$ is a complex function of various parameters such as temperature, aerosol water content, and chemical composition of the aerosol that influence both uptake of N_2O_5 into the particles (McDuffie et al., 2018a) and the subsequent aqueous phase chemistry leading to the formation of $ClNO_2$ (McDuffie et al., 2018a). The uptake of N_2O_5 (Reaction R4) and the reaction of NO_3 with VOCs (Reaction R5) constitute an overall loss term for the sum of NO_3 and N_2O_5, because the fast equilibrium between NO_3 and N_2O_5. HNO_3 formation by Reaction R4 is an important atmospheric sink for atmospheric nitrogen oxides in the lower atmosphere, because HNO_3 photolysis is slow so that most of the produced HNO_3 does not reform NO_2, but is removed from the atmosphere by deposition (Brown and Stutz, 2012). During the daytime, NO_3 is destroyed by photolysis or by reaction with nitric oxide (NO). The thermal equilibrium between NO_3 and N_2O_5 thus leads to a rapid depletion of N_2O_5 at day. Therefore, significant concentrations of N_2O_5 (the precursor of $ClNO_2$) are usually only present at night.

Previous studies reporting $ClNO_2$ measurements in North America (Osthoff et al., 2008;Thornton et al., 2010;Mielke et al., 2011;Wagner et al., 2012;Young et al., 2012;Mielke et al., 2013;Riedel et al., 2013;McDuffie et al., 2018b;McNamara et al., 2020), Asia (Tham et al., 2016;Wang et al., 2016;Liu et al., 2017;Wang et al., 2017a;Wang et al., 2017b;Le Breton et al., 2018;Yun et al., 2018;Zhou et al., 2018;Yan et al., 2019;Jeong et al., 2019;Lou et al., 2022) and Europe (Phillips et al., 2012;Bannan et al., 2015;Priestley et al., 2018;Sommariva et al., 2018) have shown that $ClNO_2$ is present in various environments even at a distance from the coast, indicating that other sources of chloride than sea spray contribute to the availability of chlorine for the formation of $ClNO_2$. Observed mixing ratios of $ClNO_2$ in the atmosphere range from a few hundred pptv to several ppbv exhibiting significant spatial and temporal variations.

Despite the large variation in $ClNO_2$ concentrations and its potentially important contribution to photochemistry, systematic investigations of seasonal differences of $ClNO_2$ concentrations are sparse, because $ClNO_2$ is not regularly measured at monitoring stations, but during intensive field campaigns, which last typically only a few weeks. Sommariva et al. (2018) reported $ClNO_2$ measurements at three different locations in the United Kingdom in all four seasons showing a clear seasonal variation with maximum concentrations in spring and winter. Another study by Mielke et al. (2016) reporting the seasonal behavior of $ClNO_2$ in Calgary, Canada, also showed maximum mixing ratios of $ClNO_2$ of up to 330 pptv in winter and spring.

The large variability of $ClNO_2$ concentrations in the atmosphere is due to the complexity of its formation mechanism (Reactions R2 – R5) and the variability of its precursor concentrations. Assuming steady state for the sum of NO_3 and N_2O_5 concentrations, the following relationship holds

$$\frac{d[NO_3+N_2O_5]}{dt} \cong 0 = k_2[NO_2][O_3] - k_{NO_3}[NO_3] - k_4[N_2O_5] \quad \text{(Eq. 1)}$$

where k_{NO_3} represents the pseudo first-order rate constant for NO_3 loss mainly dominated by reactions with atmospheric VOCs (Reaction R5) at night with no fresh NO emissions. Considering the thermal equilibrium between NO_3 and N_2O_5, the $[NO_3]$ can be replaced by $[N_2O_5]/(K_{eq}(T)[NO_2])$ where $K_{eq}(T)$ is temperature dependent and equals to the ratio of the reaction rate constants of the thermal equilibrium, i.e. k_{3a} to k_{3b} (Reaction R3a and b). Equation 1 can be solved for

$$[N_2O_5] = \frac{K_{eq}(T)[NO_2]}{k_{NO3}+K_{eq}(T)[NO_2]k_4} \cdot k_2[NO_2][O_3] \quad \text{(Eq. 2)}$$

The production rate of $ClNO_2$ is then

$$P_{ClNO2} = \varphi \cdot k_4 \cdot [N_2O_5] = \varphi \cdot \left(\frac{K_{eq}(T)[NO_2]k_4}{k_{NO_3}+K_{eq}(T)[NO_2]k_4}\right) \cdot k_2[NO_2][O_3] \quad \text{(Eq. 3)}$$

A production efficiency ε for $ClNO_2$ can be defined from this relationship

$$\epsilon_{ClNO2} = \frac{P_{ClNO2}}{k_2[NO_2][O_3]} = \varphi\left(\frac{K_{eq}(T)[NO_2]k_4}{k_{NO3}+K_{eq}(T)[NO_2]k_4}\right) \quad \text{(Eq. 4)}$$

It represents the formation rate of $ClNO_2$ from aerosol per NO_3 produced by the reaction of NO_2 with O_3 in the gas phase. Equations Eq. 3 and Eq. 4 describe the expected influences on the $ClNO_2$ formation by its precursors NO_2 and O_3, by temperature and NO_2 controlling the equilibrium between NO_3 and N_2O_5, and the competing loss reactions of NO_3 and N_2O_5 via Reactions R5 and R4, respectively. φ is an

additional variable depending on the properties of the aerosol and specifically on its chloride content, as mentioned above.

This study presents $ClNO_2$ measurements performed during the Jülich Atmospheric Chemistry Project (JULIAC) campaign in three seasons (i.e. winter, summer, and autumn 2019). The JULIAC campaign aimed to investigate the seasonal and diurnal variations of the atmospheric oxidation capacity at a rural site that is typical for mid-west Europe. To minimize the impact of emissions from local sources, the air was drawn from 50 m above ground ensuring that air is sampled from above the surface layer during nighttime and flowed through the large environmental chamber SAPHIR at Forschungszentrum Jülich, Germany. In this work, the seasonal variation of $ClNO_2$ concentrations and its formation are investigated. As mentioned above, previous studies have demonstrated that $ClNO_2$ concentrations show significant seasonal variations (Mielke et al., 2016; Sommariva et al., 2018). However, intensive seasonal measurements in central Europe, to our knowledge, have not been performed so far. Given the ubiquitous nature of $ClNO_2$ and its importance to enhance atmospheric oxidation processes, more detailed studies are needed to broaden our knowledge of atmospheric $ClNO_2$ levels, its seasonal behavior and its distribution in environments with different chemical conditions. In addition, this work presents empirical production efficiencies of $ClNO_2$ determined from the nighttime measurements of $ClNO_2$, NO_2 and O_3 and analyzed for their seasonal variations and origin of air masses, a prerequisite to understand the contribution of $ClNO_2$ to radical photochemistry under the chemical and meteorological conditions encountered in this campaign. Finally, a chemical box model is used here to understand the dependence of $ClNO_2$ formation and production efficiency on the observed nocturnal O_3 and NO_2 concentrations. The measurements and analysis presented in this paper help to illustrate the seasonal variability of $ClNO_2$ concentrations and shed light on the factors that control its production in different seasons.

2 Methods

2.1 The JULIAC campaign

The JULIAC campaign was conducted in 2019 in the atmospheric simulation chamber SAPHIR on the campus of Forschungszentrum Jülich, which is located at a rural site in Germany (50.91° N, 6.40° E). The SAPHIR chamber consists of a double-wall Teflon film (volume: (277 ± 3) m^3) (Bohn et al., 2005;Rohrer et al., 2005). Its high volume to surface ratio (1 m^2/m^3) minimizes air-surface interactions within the chamber. The time scale of mixing is about 1 minute ensured by two fans that are operated inside the chamber.

During this study, ambient air was drawn from 50 m height above ground into the chamber (Fig. S1, Supporting Information). At this height, the air is expected to be decoupled from the surface layer during the night, so that the air composition is not directly impacted by sources at the ground or deposition of trace gases to the Earth's surface (Section 3.3). The inlet line (SilcoNert® coated stainless steel, inner diameter: 104 mm) was mounted at a tower (JULIAC tower) next to the chamber. A fast flow rate of 660 m^3/h resulted in a residence time of the air inside the inlet line of approximately 4 s. The short residence time and the inertness of the Silconert coating of the inlet line minimized loss and chemical changes of the air before entering the SAPHIR chamber. The potential loss of trace gases in the inlet line was tested for O_3, NO, NO_2, and CO and was found to be less than 5%.

Instruments could either sample air directly from the inlet line or the chamber volume. In the latter case, part of the total air drawn through the inlet at the JULIAC tower flowed through the SAPHIR chamber with a flow rate of 250 m^3/h that was controlled by a three-way valve right upstream of the injection point into the chamber. The remaining part was vented. The residence time of sampled ambient air inside the SAPHIR chamber was 1.1 hours calculated from the measured flow rate and the chamber volume. Sampling air from the large volume of the SAPHIR chamber has the advantage that short-term variations of trace gas concentrations flowed into the chamber for example due to local emissions or fast changes of air masses are smoothed.

The JULIAC campaign consisted of four intensive measurement periods in winter (14 January to 10 February 2019), spring (08 April to 05 May 2019), summer (05 August to 01 September 2019), and autumn (28 October to 24 November 2019). During these parts of the campaign, a large set of instruments sampled air from the chamber. In addition, between each intensive measurement period, a limited set of instruments for the detection of $ClNO_2$, O_3, NO, NO_2, OH reactivity, and VOCs continued measuring directly from the inlet line at the JULIAC tower (Fig. S1, Supporting Information).

2.2 Instrumentation

A large set of instruments was deployed during the JULIAC campaign. In this work, the focus is on measurements that are relevant to study the chemistry of $ClNO_2$.

$ClNO_2$ was measured by a chemical ionization mass spectrometry (CIMS) instrument from Leicester University (THS Instruments LLC, GA, USA) operated in negative ion mode using iodide (I^-) as reagent ion. $ClNO_2$ was detected at the mass to charge ratios (m/z) of 208 and 210 amu, corresponding to the two isotopes of the $[I \cdot ClNO_2]^-$ ion clusters as described in Sommariva et al. (2018).

The CIMS instrument was calibrated by standard additions of $ClNO_2$ generated by flowing humidified air containing Cl_2 (from a cylinder containing a mixture of 5 ppmv (±5%) Cl_2 in N_2, Linde AG) over a salt bath containing a 1:1 mixture of NaCl and $NaNO_2$ (Sommariva et al., 2018). The resulting $ClNO_2$ concentration in the air was determined by measuring the NO_2 concentration after thermally decomposing $ClNO_2$ to Cl and NO_2 in a glass tube heated to a temperature of 400 °C. The NO_2 concentrations were measured using a commercial NO_2 analyzer that makes use of the cavity attenuated phase-shift method (CAPS, T500U, Teledyne API). The accuracy of NO_2 measurements by this analyzer is ±5%. The overall accuracy of the $ClNO_2$ calibration is ±17%; the precision of $ClNO_2$ measurements is 13% with a 2-σ detection limit of 5.6 pptv at a 1-minute time resolution.

The CIMS detection sensitivity depends on humidity because iodide ions form clusters with water ($I\cdot(H_2O)^-$). The water-iodine cluster is a more efficient reagent ion for producing $I\cdot(ClNO_2)^-$ clusters than the I^- ion (Kercher et al., 2009). The dependence of the sensitivity on humidity was characterized with calibration experiments by varying the mixing ratios of water vapor. These experiments show that the sensitivity of the instrument for the detection of $ClNO_2$ decreases by 19% per 1% water vapor mixing ratio (Fig. S2, Supporting Information), when the signal is normalized to the $I\cdot(H_2O)^-$ cluster signal (m/z = 145). Calibrations of the instrument were performed during each measurement period using comparable average humidity to that of the ambient air. The variability of the sensitivity due to the changes in humidity in each 4-week long measurement period was less than ±5%. This is within the range of reproducibility of calibration measurements. Therefore, the sensitivity was not corrected for the humidity effect for individual data points, but an average sensitivity value was applied to all data from the entire measurement period. The uncertainty due to the humidity dependence of the sensitivity and the reproducibility of the calibration adds to the overall accuracy of $ClNO_2$ measurements increasing the value to ±27%.

Photolysis frequencies inside the SAPHIR chamber were calculated from the actinic flux measured outside the chamber and corrected for the reduction of radiation by shading effects and the transmission of the Teflon film (Bohn et al., 2005). Ozone was detected by a UV photometer (model O342M, Ansyco). Nitric oxide (NO) was measured by a chemiluminescence instrument (780TR, Eco Physics) that was also used to detect NO_2 by conversion of NO_2 to NO in a blue-light photolytic converter upstream of the NO analyzer. For the period after 01 December 2019, NO_2 was measured by an instrument using the iterative cavity enhanced differential optical absorption spectroscopy method (ICAD1005, AirYX). The NO_2 measurements from the two instruments agreed well within 5%, when both instruments measured concurrently. Water vapor and carbon monoxide (CO) concentrations were measured by a cavity ring-

down instrument (G2401, Picarro). NO_3 and N_2O_5 were measured by a custom-built cavity ring-down instrument that is similar to the one described in Wagner et al. (2011).

Particle number concentration (for particles with a diameter > 5 nm) and size distribution (for particles with a diameter between 10 and 1000 nm) were measured by a condensation particle counter (model 3787, TSI) and a scanning mobility particle sizer (model 3080, TSI), respectively. The aerosol surface area (S_a) was calculated based on the particle number and geometric diameter in each size bin. The chemical composition of particles was analyzed by an aerosol mass spectrometer (HR-TOF-AMS, Aerodyne).

Temperature and pressure of the ambient air were measured inside the chamber and also outside the chamber at different heights (2 m, 20 m, 30 m, 50 m, 80 m, 120 m) by sensors mounted at a meteorological tower located approximately 200 m away from the SAPHIR chamber.

2.3 Comparability of measurements from the chamber and the inlet line

Air was sampled from 50 m above the ground from the top of the JULIAC tower at all times of the campaign (Fig. S1, Supporting Information). However, $ClNO_2$ concentrations were determined in the air from either one of the two sampling points during the different periods of the campaign.

During the intensive measurement periods (i.e. in February, August, and November), air was directly sampled from the SAPHIR chamber. During other times, air was sampled from the inlet system of the chamber at the JULIAC tower. In both cases, measured concentrations are representative for the air from 50 m height. In the case of sampling from the chamber, concentrations are averaged due to the 1-hour residence time of air in the chamber.

To make data derived from both sampling points comparable, $ClNO_2$ concentrations measured inside the chamber ($C_{chamber}$) were converted to equivalent concentrations at the tip of the JULIAC inlet system (C_{50m}). This can be achieved from the differential equation of concentrations taking into account dilution with the flow rate (k_{flow}) and loss ($L_{chamber}$) and production ($P_{chamber}$) inside the chamber:

$$\frac{dC_{chamber}}{dt} = k_{flow}(C_{50m} - C_{chamber}) + P_{chamber} - L_{chamber} \quad \text{(Eq. 5)}$$

The concentration in the incoming air can be iteratively determined from the time series of measured concentrations inside the chamber, if loss and production processes can be quantified. The other species used in this work (e.g. O3, NOx, etc.) were measured both at the tip of the JULIAC inlet and inside SAPHIR. Unless otherwise specified, the measurements presented in this work were taken at the tip of the JULIAC inlet, or corrected using Eq 5.

Production of $ClNO_2$ from the heterogeneous reaction of N_2O_5 on particles is expected to be negligible on the time scale of the residence time of air in the chamber for conditions of the JULIAC campaign. Chamber wall interaction could be relevant because the surface area of the Teflon film is 10^6 $\mu m^2/cm^3$, i.e. several orders of magnitude larger than the surface area of ambient aerosol experienced in this campaign, which were on the order of tens to hundreds of $\mu m^2/cm^3$. To quantify potential chamber related loss and production processes, chamber characterization experiments were conducted (Section 3.1). They were analyzed by using a chemical box model, in which loss and production rates were adjusted to reproduce measured $ClNO_2$ concentrations during these experiments. Temperature, relative humidity, pressure, photolysis frequencies, and dilution rates determined from the air replenishment flow rate were constrained to measurements in the model. The conversion of N_2O_5 to $ClNO_2$ via surface reactions (Reaction R6) and the loss reactions of $ClNO_2$ on the chamber wall (Reaction R7) were included in the model assuming pseudo-first order processes:

$$N_2O_5 + wall \rightarrow ClNO_2 \quad \text{(R6)}$$

$$ClNO_2 + wall \rightarrow products \quad \text{(R7)}$$

In addition, the chemical loss of $ClNO_2$ via photolysis (Reaction R1) was considered. The results of these experiments and the model analysis are discussed in Section 3.1.

3 Results and Discussion

3.1 Chamber effects on measured $ClNO_2$ concentrations

Two types of experiments were performed to characterize the chamber properties with respect to wall interaction of NO_3, N_2O_5, and $ClNO_2$. In these chamber characterization experiments, only a small replenishment flow of pure synthetic air compensated for leakages and extraction of air by instruments. This led to a low dilution of trace gases with a rate that is equivalent to a lifetime of 17 hours in contrast to the 1-hour lifetime during the operation of the chamber in the JULIAC campaign.

Three experiments were conducted (05, 06, and 07 February 2019) to test whether $ClNO_2$ was exclusively lost by photolysis in the chamber or whether other processes, such as wall loss, contributed to the $ClNO_2$ removal. These experiments started with flowing ambient air through the SAPHIR chamber during the night like in the operational mode of the JULIAC campaign (Section 2.1). The high flow was stopped before sunrise (around 06:00 UTC) and the small replenishment flow was started. The evolution of trace gas concentrations was observed until around 12:00 UTC while the air was exposed to sunlight. The N_2O_5

concentration decreased rapidly to zero after sunrise and thus no further $ClNO_2$ could be produced from N_2O_5 conversion and $ClNO_2$ concentrations also decayed during the morning.

Measured concentrations are compared to calculation using a chemical box model (Section 2.3) considering losses of $ClNO_2$ by dilution, photolysis, and potential wall loss. Whereas loss rates for dilution and photolysis are constrained to measurements, the wall loss rate constant is adjusted to match observed $ClNO_2$ concentrations. This results in a wall loss rate constant for $ClNO_2$ of 2.1×10^{-5} s^{-1}. This value is on the same order of magnitude as the loss rate constant of $ClNO_2$ due to photolysis (4.1×10^{-5} s^{-1} at noon) and dilution (1.5×10^{-5} s^{-1}) for the experimental conditions of the characterization experiments. Due to the higher chamber flow rate used during the JULIAC campaign, the dilution rate is an order of magnitude higher (2.5×10^{-4} s^{-1}) than during the characterization experiments. Therefore, the wall loss rate is only 8% of the dilution rate, and thus can be neglected in the further data analysis.

Additional three experiments were performed to characterize potential $ClNO_2$ formation from heterogeneous reactions of N_2O_5 on the chamber wall. In these experiments (18 September, 18 October, and 19 November 2019), NO_2 and O_3 were added into the dark chamber filled with pure, dry, or humidified synthetic air. These experiments lasted for about 10 hours to observe the decay of NO_2 and O_3 concentrations and the accumulation of $ClNO_2$.

Fig. 1 shows measured concentrations for the experiments performed on 19 November. In this experiment, the chamber air was humidified (RH=60%) and 28 ppbv of NO_2 and 80 ppbv of O_3 were injected to produce NO_3 and N_2O_5. NO_3 mixing ratios were below the limit of detection (about a few pptv) of the cavity ring-down instrument.

N_2O_5 measurements reached maximum mixing ratios of 0.17 ppbv shortly after the O_3 injection and decreased afterward (Fig. 1). Also, $ClNO_2$ production was observed shortly after the ozone addition, when N_2O_5 was present. Because the air was particle-free, one possible explanation for the formation of $ClNO_2$ is heterogeneous reaction of N_2O_5 on the chamber wall that may contain chloride, which could have been deposited, for example, during previous experiments with ambient air.

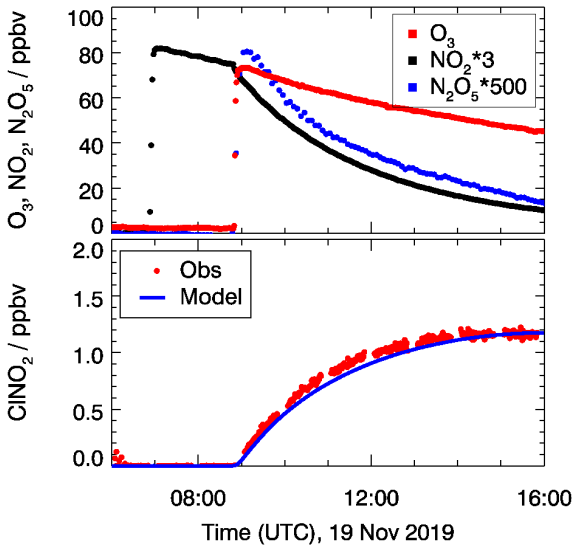

290

291 **Figure 1.** Chamber experiment to characterize $ClNO_2$ production from N_2O_5 conversion on the chamber
292 wall in the dark on 19 November 2019. $ClNO_2$ concentrations are compared to model calculations taking
293 conversion from N_2O_5 to $ClNO_2$ (Reaction R6) into account. A reaction rate constant of 8.2×10^{-6} s^{-1} is
294 required to reproduce measured $ClNO_2$ concentrations.

295 The values of the conversion rates from N_2O_5 to $ClNO_2$ (Reaction R6) that are required to match the
296 measured $ClNO_2$ concentrations in the model calculations are $k_{R6} = 4.0 \times 10^{-6}$ s^{-1}, 2.0×10^{-6} s^{-1}, and $8.2 \times$
297 10^{-6} s^{-1} for the experiments on 18 September, 18 October and 19 November 2019, respectively.

298 During the JULIAC campaign, however, the potential contribution of $ClNO_2$ formation from N_2O_5
299 conversion on the chamber film was negligible. Taking the typical nocturnal N_2O_5 mixing ratio of about
300 50 pptv, the expected $ClNO_2$ production rate from N_2O_5 conversion on the chamber wall was about 1.5
301 pptv/h using the upper limit value of k_6 derived from the characterization experiments. This is less than
302 1% of the ambient $ClNO_2$ mixing ratio of up to several hundred pptv in the ambient air that is flowed into
303 the chamber. Therefore, no corrections are needed for the interpretation of $ClNO_2$ measurements in the
304 chamber.

305 Overall, the results of the characterization experiments allow to simplify the back-calculation of the
306 $ClNO_2$ concentrations in the sampled air from measured concentrations in the chamber (Eq. 5). The
307 chemical production rates and the deposition rates for $ClNO_2$ and N_2O_5 on the chamber walls can be
308 neglected and only photolysis needs to be considered as a destruction process for $ClNO_2$ during the
309 daytime. For nighttime conditions, $ClNO_2$ concentrations in the incoming air can be determined solely
310 from the flow rate and the measured $ClNO_2$ concentration inside the chamber.

3.2 Overview of measurements

In order to determine the origin of air masses sampled at the measurement site, back trajectories were calculated using the HYSPLIT model (Stein et al., 2015) for every second hour. They were calculated for a height of 50 m above the ground and started 48 hours earlier before the air arrived at the measurement site. Calculations for different heights (500 m and 1000 m) gave similar results as the trajectories calculated for a height of 50 m. To extract information about the relation between the source of air masses and the measurements, the cluster analysis tool of the HYSPLIT model was used, which classified the trajectories into two groups (Fig. 2).

Trajectories showed most often prevailing long-distance transport of air masses from the southwest, from which they traveled hundreds of kilometers from the Atlantic Ocean (approximately 1000 km away from the measurement site) within 48 hours. These air masses were likely influenced by marine and continental emissions as they crossed over northern France and Belgium. They are referred to hereafter as belonging to the long-range transport group. The other group of trajectories did not show a prevalent direction but shared the common feature that these air masses circulated over the cities nearby the measurement site, e.g. Cologne, Düsseldorf, and Frankfurt (Fig. 2). These air masses are therefore influenced by regional emission sources and are referred in the following to belong to the regional transport group.

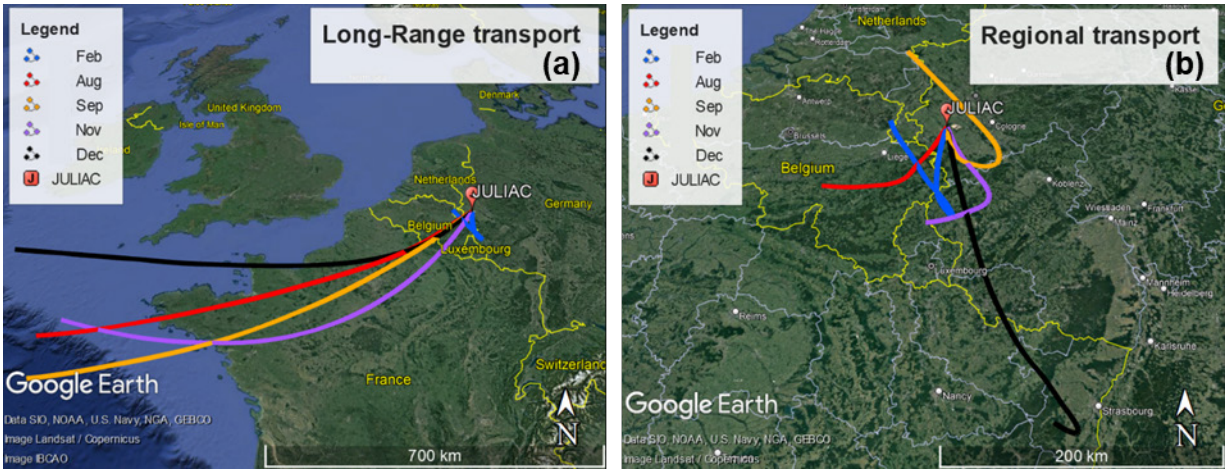

Figure 2. Results of the HYSPLIT cluster analysis of 48h back trajectories for the different measurement periods. (a) Trajectories from air masses originating from long-range transport for each period. (b) Trajectories from air masses from regional transport. © Google Maps 2022.

Fig. 3 shows mean diurnal profiles of $ClNO_2$, NO_2, O_3 concentrations, and photolysis frequencies of $ClNO_2$ in February, August, September, November, and December 2019, if measurements are split into 2 groups depending on the type of back trajectory associated to the measurement at that time. The complete

time series of measurements used for the analysis in this work are shown in Fig. S3-S7 (Supporting Information).

In all cases, the diurnal profiles of $ClNO_2$ showed an increase of concentration after sunset as can be expected from its chemical production during the night. Maximum concentrations were reached around midnight and $ClNO_2$ concentrations remained relatively constant until sunrise, when they started to decrease due to its photolysis.

The reaction chain to produce $ClNO_2$ at the night starts with the reaction of NO_2 and O_3. The median observed O_3 showed little diurnal variation in the cold seasons (February, November, and December) (Fig. 3). At this time of the year, the O_3 level was generally higher in long-range transported air (30 - 40 ppbv O_3) compared to regionally influenced air (15 – 20 ppbv O_3), for which ozone depletion by urban NO emissions was likely more important due to fresh emissions. During summer when photochemistry was most active (August, September), the median O_3 concentrations were considerably higher in regionally influenced air. Ozone mixing ratios in summer showed distinct diurnal profiles with noontime maxima of 80 ppbv in August and 40 ppbv in September, and nighttime values between 20 and 30 ppbv. In contrast, long-range transported air exhibited a less pronounced diurnal variation in the O_3 concentration and mixing ratios were often only between 20 and 40 ppbv. The high summertime ozone concentrations in regionally-transported air is likely due to fresh emissions of NO and VOCs, which are photochemically converted to O_3.

The influence of fresh emissions from nearby sources is also visible in the measured NO_2 concentrations, which were higher in regional air masses compared to concentrations in long-range transport air masses during the entire year. For regionally-transported air masses, average nocturnal NO_2 mixing ratios were around 10 ppbv in all measurement periods, except in December, when mixing ratios were lower with values of about 5 ppbv. In the night, median NO_2 concentrations in long-range transported air masses were generally lower than 5 ppbv in all seasons.

The age of the airmass could play a role in the observed levels of $ClNO_2$ due to the impact on NO_2 and O_3 concentrations, and hence on $ClNO_2$. As shown in Fig. 2, regionally transported air masses spend more time over urban areas picking up anthropogenic emissions (indicated by high NO_2 mixing ratios). They also have more time for the photochemical processing of pollutants compared to the long-range transported air masses. In the cold months (February, November, and December), long reaction times would lead to lower O_3 concentrations for the regional air masses due to the titration by anthropogenically emitted NO compared to conditions in August and September when photochemical ozone production is more efficient than the titration effect.

The nocturnal $ClNO_2$ concentrations were consistently lower in air masses from long-range transported air compared to regional transported air in nearly all seasons except again in December. The maximum median nighttime values were around 0.2 ppbv in long-range transported air and around 0.5 ppbv in air masses from regional transport (Fig. 3). Only in December, no significant dependence of the $ClNO_2$ concentration on the origin of air masses was observed.

Maximum $ClNO_2$ mixing ratios of 1.6 ppbv (15-min average), which were observed at 03:00 UTC on September 15 in the JULIAC campaign (Fig. S5, Supporting Information), are comparable to observations in other field campaigns. In Europe, high $ClNO_2$ mixing ratios have also been observed during summer in several field campaigns, in which $ClNO_2$ was measured: 0.8 ppbv near Frankfurt, Germany (Phillips et al., 2012), 0.8 ppbv in London, UK (Bannan et al., 2015) and 1.1 ppbv in Weybourne, UK (180 km northeast of London, (Sommariva et al., 2018)).

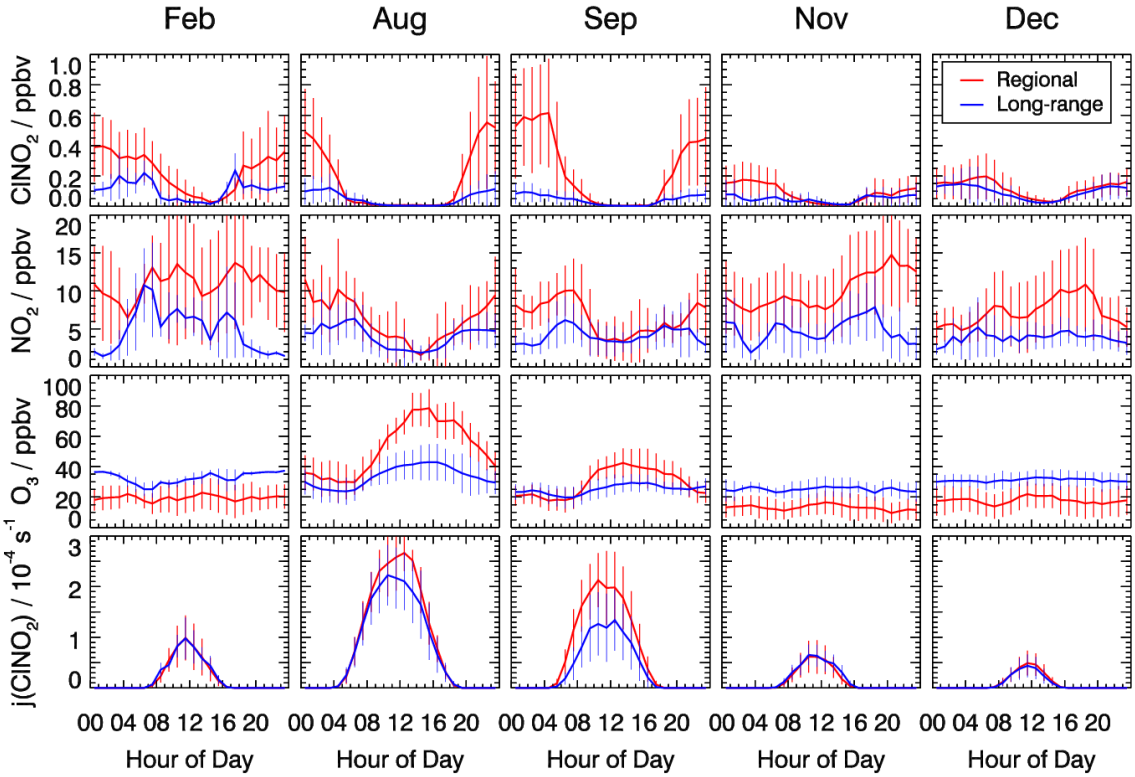

Figure 3. Mean diurnal profiles of $ClNO_2$, NO_2, and O_3 concentrations, and $ClNO_2$ photolysis frequencies. Trace gas concentrations were measured in the inflowing air or values measured inside the chamber were used to back-calculate concentrations in the inflowing air. Data are 1-h average values with error bars denoting 1σ standard deviations.

The seasonally varying photolysis frequencies of $ClNO_2$ showed diurnal noontime maxima of 0.4×10^{-4} s^{-1} in winter and 2.5×10^{-4} s^{-1} in summer. Sunlight lasted longest in summer and photolysis frequencies were sufficiently high to destroy all $ClNO_2$ before midday. In contrast, daytime $ClNO_2$ concentrations remained significantly above zero (around 30 pptv) in the cold seasons, because the maximum photolysis frequencies were a least a factor of 2 lower than in summer and the duration of daylight was not long enough to deplete all $ClNO_2$. Similar results were observed in wintertime measurements of $ClNO_2$ by Sommariva et al. (2021).

Seasonal differences in $ClNO_2$ concentrations observations in this work can be compared to the seasonal variations reported for measurements performed in Leicester, UK (Sommariva et al., 2018). In Leicester, the highest $ClNO_2$ mixing ratio of 0.73 ppbv was observed in February, when also NO_2 mixing ratios were highest with values of 43 ppbv. The seasonality of $ClNO_2$, NO_2, and O_3 observed during the JULIAC campaign was different from the seasonality observed in Leicester. In this work, the highest $ClNO_2$ concentrations were experienced in summer, when the air was influenced by emissions from nearby cities (regional transport) resulting in high NO_2 and O_3 concentrations. The different seasonal behavior in Jülich and Leicester suggests that the controlling factor for the production of $ClNO_2$ could have been different in the two locations (Section 3.5).

3.3 Influence of the nocturnal vertical stratification of air on $ClNO_2$ concentrations

The $ClNO_2$ measurements presented in this work were obtained in air sampled at a height of 50 m above ground (Section 2). While there is a well-mixed layer due to convection during the day, the cooling of the ground results in weak convection of air after sunset leading to stratification of the air in the night.

In general, layers can be identified by the vertical profile of the potential temperature. In the night, a stable surface layer (typically <20 m height) is expected to be formed, in which emissions from the ground are trapped. A weakly stable nocturnal boundary layer is on top of the surface layer (NBL, typically in the height range between 20 m and 200 m) and a residual layer that is fully decoupled from the ground (typically height >200 m) (Brown et al., 2007). Because the tip of the inlet of the SAPHIR-JULIAC inlet system was 50 m above the ground, it was most often located within the nocturnal boundary layer and thus impact of surface emissions in the sampled air is expected to be small.

This was particularly the case in the cold seasons (Feb., Nov., and Dec.) suggesting that most of the nighttime measurements presented in this work are representative of conditions in the NBL. Similar conditions were encountered in the summer during nights with low wind speed and cloudless conditions. However, in 8 out of 30 nights from 20 August to 20 September, the sampled air at 50 m height was

temporarily influenced by surface air. Indicators were, for example, observed enhancements of the NO and CO concentrations, and reduced mixing ratios of $ClNO_2$.

An example of such an event is shown in Fig. 4 which presents measurements from the night of 21 to 22 August 2019. After sunset (around 19:00 UTC), a stable surface layer was formed as indicated by a positive vertical temperature gradient in the lowest 20 m (Fig. 4a). Until 22:00 UTC, the surface layer height increased and developed a strong temperature inversion at 30 m height. Above the surface layer, the temperature gradient was slightly positive up to a height of 80 m. It is expected that for the conditions until about 22:00 UTC, the measured air at 50 m height was not influenced by surface emissions. During this time, $ClNO_2$ mixing ratios increased continuously to 1.5 ppbv due to chemical production. After 22:30 UTC, $ClNO_2$ decreased to 0.5 ppbv until 0:00 UTC. The decrease coincided with an increase in wind speed from below 2 m/s at 23:00 UTC to about 4 m/s at 0:00 UTC. This might be related to the phenomenon of "nocturnal jets" that can produce high wind speeds at low altitudes already in a range of 50 m. The elevated wind speed and change of wind direction indicate air mass came down the Rur valley from Düren, a small city 10 km away from the site. At the same time, the steep temperature gradient of the inversion at 30 m disappeared and most likely facilitated entrainment of surface air with lower $ClNO_2$ concentration. This assumption is supported by an enhanced NO mixing ratio of 0.2 ppbv observed shortly before midnight, indicating ground emissions (Fig. 4(b)). At the same time, the NO_2 mixing ratio increased and the O_3 mixing ratio decreased by a similar amount (10 ppbv) likely due to the chemical titration of O_3 by freshly emitted NO (Fig. 4(c)). The drop of $ClNO_2$ may have been caused by the lower $ClNO_2$ production in the surface layer, because N_2O_5 concentrations were low due to N_2O_5 and NO_3 loss on surfaces and chemical loss in reactions with NO and organic compounds that have emission sources on the ground. At later times in this night, $ClNO_2$ mixing ratios increased again to a value of 1.3 ppbv at 01:00 UTC (Fig. 4(b)), when the air was again sampled from within the nocturnal boundary layer, where loss processes are expected to be smaller compared to the surface layer.

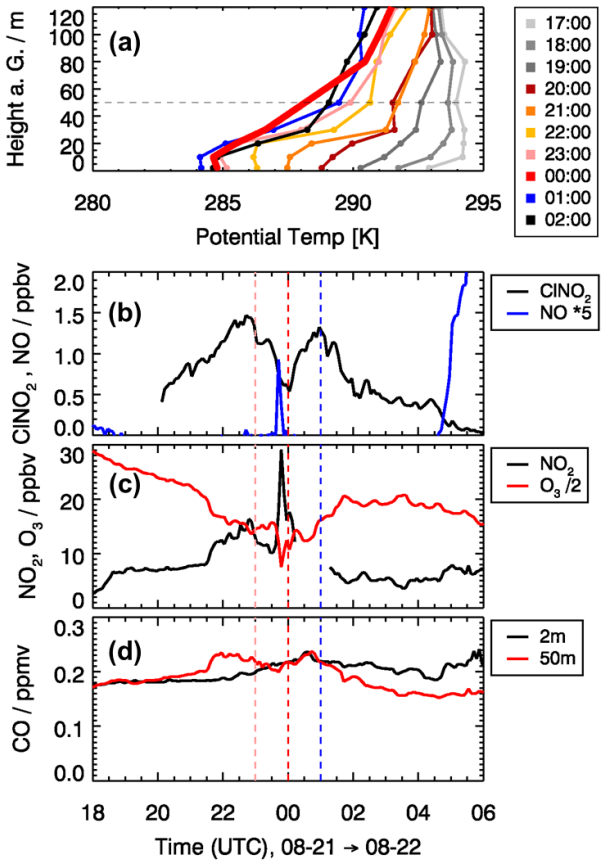

437

438 **Figure 4.** Impact of the vertical structure of air masses during the night from 21 to 22 August on observed
439 trace gas concentrations. (a): Vertical profiles of the potential temperature derived from temperature
440 measurements at different heights (2 m, 10 m, 20 m, 30 m, 50 m, 80 m, 100 m, 120 m). (b)-(d): $ClNO_2$,
441 NO, NO_2, O_3, and CO mixing ratios sampled at 50 m height with the JULIAC-SAPHIR inlet system. CO
442 mixing ratios were also measured at a height of 2 m. Colors of vertical lines correspond to colors of the
443 vertical profiles of the potential temperature.

444 The median diurnal profiles presented in Section 3.2 include all measurements. The different behavior
445 observed during the night, when air was temporarily impacted by surface interaction only constitute a
446 small fraction of the measurement time. To quantify the influence of surface interactions, elevated NO
447 concentrations at the sampling point can be used. For more than 90% of the time, measured NO mixing
448 ratios are lower than 0.1 ppbv (Fig. S8, Supporting Information) indicating that air masses were typically
449 little influenced by surface emissions. Therefore, it can be assumed that the sampling point was most
450 often located in the nocturnal boundary layer. Median values further analyzed in this work are
451 representative of conditions in the nocturnal boundary layer.

3.4 $ClNO_2$ production efficiency

The $ClNO_2$ production efficiency (ε) defined in Eq. 4 is affected by (1) the thermal equilibrium between NO_3 and N_2O_5, (2) the loss of NO_3 + N_2O_5 by reaction of NO_3 with VOCs and heterogeneous uptake of N_2O_5 on the aerosol surface, and (3) the yield of $ClNO_2$ from the heterogeneous reaction of N_2O_5. The value of the production efficiency cannot be simply calculated because the required parameters along the trajectory of the studied air mass are not known. Instead, a mean value of ε is estimated empirically from the observed nocturnal increase of the $ClNO_2$ concentration at the measurement site and the corresponding integrated NO_3 production rate. This approach assumes that there are no significant nocturnal $ClNO_2$ losses in the studied air.

$$\varepsilon_t = \frac{([ClNO_2]_t - [ClNO_2]_{t0})}{\int_{t0}^{t} P(NO_3)_{(t)} dt} \quad \text{(Eq. 6)}$$

For the calculation of the efficiency (Eq. 6) from measured $ClNO_2$ concentrations, the $ClNO_2$ concentration at sunset ($[\mathrm{ClNO_2}]_{t0}$) is subtracted, because this fraction of $ClNO_2$ can be assumed to be produced in the previous night. This correction is important, especially for conditions in winter and late autumn, when tens of pptv of $ClNO_2$ were observed before sunset because of the long chemical lifetime of $ClNO_2$ under these conditions (Fig. 3).

An accurate calculation of the integrated NO_3 production rate would require the knowledge of the NO_2 and O_3 concentrations while the air mass is being transported, but the exact concentrations are only known at the location of the JULIAC tower. Therefore, it is necessary to make assumptions about the history of the air mass. For simplification, it is here assumed that the airmass arriving at the JULIAC site is homogeneous along the trajectory after sunset. This assumption requires that the consumption of NO_2 by reaction with O_3 is small over the integration time and that the chemical composition of the studied air remains undisturbed by mixing with air masses containing different trace gas concentrations. The latter assumption seems reasonable when the air is sampled above the nocturnal surface layer which was largely the case during the JULIAC campaign (Section 3.3). For these assumptions, the integrated NO_3 radical production P(NO_3) can be calculated from the measured NO_2 and O_3 concentrations at the measurement site and the reaction rate constant (k_2) of their reaction. The value of the reaction rate constant is taken from recommendations by IUPAC (Atkinson et al., 2004). Therefore, the production rate of NO_3 radical can be substituted by the reaction rate of NO_2 and O_3 and Eq. 6 is rewritten as following:

$$\varepsilon_t = \frac{[\mathrm{ClNO_2}]_t - [\mathrm{ClNO_2}]_{t0}}{\int_{t0}^{t} k_2 [\mathrm{NO_2}]_t [\mathrm{O_3}]_t dt} \quad \text{(Eq. 7)}$$

t_0 can be set to the time of sunset and the time t is stepwise increased by intervals of 5 minutes (time resolution of the dataset) to calculate the time series of the production efficiency in one night. For further analysis, the first 4 hours after sunset is averaged for each night, because $ClNO_2$ increased to its maximum concentration in most of the nights of this campaign during this time. This suggests chloride is not a limiting factor for $ClNO_2$ production. Mean values of the $ClNO_2$ production efficiency in each season can then be compared.

The $ClNO_2$ production efficiency does not show a clear seasonal behavior, but values are larger in regional transported air masses than in long-range transported air masses (Fig. 5). Mean values exhibit a similar pattern, if values are taken from the entire night or a period in the second half of the night (Fig. S9, Supporting Information).

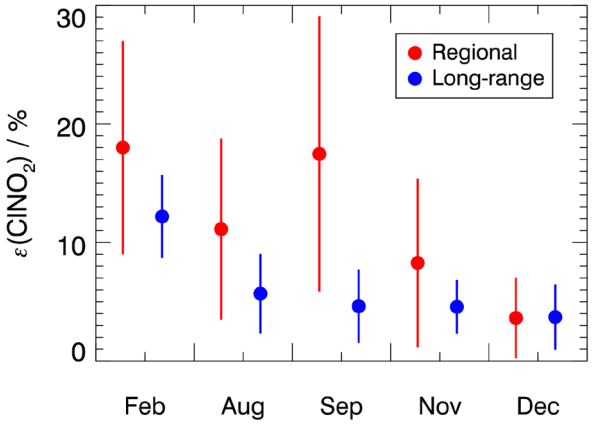

Figure 5. Mean $ClNO_2$ production efficiency for each measurement period for 4-hour average values starting after sunset. Values are calculated for air masses originating either from regional or long-range transportation. The vertical bars denote 1σ standard deviations.

For the air masses from regional transportation, the highest mean $ClNO_2$ production efficiency of (18±9) % was observed in February. This is consistent with a high NO_3 production rate due to high NO_2 concentrations (Fig. 3), as well as the low temperatures in February which favor the formation of N_2O_5. Similar $ClNO_2$ production efficiency was observed in September, although NO_2 concentrations were low. This suggests that other factors, besides the ones included in Eq. 4, contributed to the efficient production of $ClNO_2$ in regional air masses in September.

The $ClNO_2$ production efficiencies obtained in December are similar with values of (3±3) % for both regional and long-range transportation air masses. This is consistent with observations of $ClNO_2$, NO_2, and O_3 concentrations, which were also similar regardless of the origin of air masses in December (Fig.

3). In the other seasons, however, the $ClNO_2$ production efficiencies were 30 to 50% lower in air masses from long-range transportation compared to values obtained for regional air masses. This can be explained by elevated NO_2 concentrations in regional air masses, which shifts the equilibrium between NO_3 and N_2O_5 to the side of N_2O_5 and N_2O_5 and therefore facilitates the production of $ClNO_2$.

It should be mentioned that the production of $ClNO_2$ also requires the availability of particulate chloride (Reaction R4). During the JULIAC campaign, particulate chloride concentrations were measured by an aerosol mass spectrometry (AMS) instrument giving average concentrations of (0.15±0.08), (0.07±0.03), (0.07±0.06), and (0.09±0.04) $\mu g/m^3$ for measurements in February, August, September and November, respectively (measurements in December were not available, see Table S2 in the Supporting Information). The particulate chloride measurements by the AMS instrument are restricted to non-sea-salt aerosol, because the AMS was operated to measure the non-refractory particulate matters. As the measurement site is only 200 km away from the North Sea, sea salt was likely an important source of chloride in the JULIAC campaign. Thus, there was most likely more chlorine present than measured by the AMS and the observed chloride concentrations must be regarded as a low limit. Nevertheless, the high $ClNO_2$ production efficiency in the regional air masses suggests that particulate chloride was not a limiting factor for the formation of $ClNO_2$ at the measurement site (for the period of 4-hours since sunset). In the following analysis, it is assumed that the availability of particulate chloride was enough to sustain reaction R4 during this study, so $ClNO_2$ production was only dependent on the availability of its gas phase precursors (see Section 3.5).

Previous studies have reported similar values of $ClNO_2$ production efficiencies. Two field studies performed in urban environments in Canada found median values of the $ClNO_2$ production efficiency of 1.0 % (Mielke et al., 2016) and 0.17% (Osthoff et al., 2018). These low values were attributed to gas-phase loss reactions of NO_3 competing with the formation of $ClNO_2$. In addition, the authors determined significant O_3 destruction by deposition and titration in the reaction with NO in a shallow nocturnal boundary layer, which further limited the production of $ClNO_2$ (Osthoff et al., 2018). In another campaign, measurements were performed on board of a ship during a cruise in the Mediterranean Sea (Eger et al., 2019). The $ClNO_2$ production efficiency determined from these measurements was in the range between 1% and 5%, attributed to the efficient gas-phase loss of NO_3 and to the high temperature (usually >25°C) that shifted the thermal equilibrium towards NO_3, so that little N_2O_5 was expected. In contrast, the $ClNO_2$ production efficiency observed in Pasadena, U.S. (Mielke et al., 2013) was much higher than in the field studies in Canada (median value: 9.5%). These measurements were performed in the coastal boundary layer, which was characterized by high concentrations of pollutants. The authors attributed the high $ClNO_2$ production efficiency to the rapid N_2O_5 reaction with Cl that was present in

submicron aerosol particles from the redistribution of sea salt chloride as proposed by Osthoff et al. (2008).

3.5 Dependence of the $ClNO_2$ production on the availability of NO_2 and O_3

Most of the measurements taken during nighttime from a height of 50 m were not affected by fresh local emissions from the ground surface, as discussed in Section 3.2. As first approximation, it can be assumed that particulate chloride is not limiting the formation of $ClNO_2$ (Section 3.4). Therefore, the amount of $ClNO_2$ that can be formed during the night is a function of the amounts of NO_2 and O_3 available at sunset. The dependence of the $ClNO_2$ production on the availability of NO_2 and O_3 for ambient conditions is further investigated by box model calculations. This method was previously used by Sommariva et al. (2018) and a detailed description can be found in their work. In brief, the model is initialized with a matrix of initial NO_2 and O_3 concentrations. The chemical box model includes production and loss reactions of $ClNO_2$ (Reaction R1- R4, reactions rate constants are taken from the IUPAC recommendations (Atkinson et al., 2004)). $ClNO_2$ concentrations are calculated for each initial NO_2 and O_3 concentrations after 4 hours. This length of the simulation is chosen, because observed $ClNO_2$ concentrations typically reached their maximum values approximately 4 hours after sunset in the JULIAC campaign.

In the model, the efficiency of the conversion of N_2O_5 to $ClNO_2$ is assumed to be constant, with a value for the uptake coefficient of N_2O_5 of 0.01 from Bertram and Thornton (2009), and a $ClNO_2$ yield of 0.5 (Reaction R4) from Roberts et al. (2009). The aerosol surface area (S_a) measured during JULIAC was in the order of 100 $\mu m^2/cm^3$ (Table S1) and was set to this constant value in the model. Temperature was fixed at 22 °C to represent typical summer-like conditions. Hence, the pseudo-first order reaction rate constant for N_2O_5 uptake is 6.0×10^{-5} s^{-1}. Following Sommariva et al. (2018), a constant NO_3 loss rate is used to represent the typical loss of NO_3 radicals (k_{NO3}) in their reactions with organic compounds (Reaction R5). The assumed value of the NO_3 loss rate, k_{NO3}, is adjusted, so that the modelled $ClNO_2$ concentration agrees with the magnitude of the observations (Fig. S10, Supporting Information), which corresponds to an NO_3 reactivity of 0.004 s^{-1}. It should be noted that the purpose of such simplified model is to examine the idealized dependence of $ClNO_2$ on the chemical conditions, not to reproduce the measurements.

Fig. 6(a) shows the modelled $ClNO_2$ mixing ratios as a function of the initial NO_2 and O_3 concentrations at sunset. Given the chemical conditions of long-range transported air masses in summer (25 to 35 ppbv O_3 and 4 to 5 ppbv of NO_2), the model predicts $ClNO_2$ mixing ratios in the range of 0.1 to 0.16 ppbv. Because of the simplifications adopted in the modelling approach, calculated $ClNO_2$ mixing ratios tend to

underestimate the measurements the measurements, which are around 0.2-0.3 ppbv (Fig. S10). For regional air masses containing higher NO_2 mixing ratios (6 to 10 ppbv of NO_2), NO_3 production rates and therefore also calculated $ClNO_2$ mixing ratios are higher (between 0.2 and 0.4 ppbv, Fig. 6(a)). Given the position of each measurement periods in the isopleth plot, it can be concluded that all long-range transported air masses tend to be NO_2 limited while the regional transported air masses tend to be NO_2 limited in summer/autumn and O_3 limited in winter.

To further interpret the controlling factors of $ClNO_2$ production, the dependence of $ClNO_2$ production efficiency ε on NO_2 and O_3 is presented in Fig. 6 (c). The modelled $ClNO_2$ production efficiency increases with increasing mixing ratios of NO_2 but not with increasing O_3 (Fig. 6 (c)) as expected from Eq. 4, which shows that the $ClNO_2$ production efficiency is a function of multiple parameters but not of the O_3 mixing ratio. In general, the model reproduces the experimentally determined $ClNO_2$ production efficiency (as shown in Fig. 5) within the uncertainty of the calculation (30% to 40%), which is mainly due to the assumptions concerning the history of air masses (Section 3.4). However, the relatively high $ClNO_2$ production efficiency found in August and September in the regional air masses (Fig. 5) is significantly underestimated by the model. The discrepancy suggests that other processes facilitate the conversion from NO_3 to $ClNO_2$ in the regional air masses for summer-like conditions. Though the purpose of this model calculation is not to reproduce the observations, it is critical to address the related uncertainties/limitations due to the assumptions in the simplified model. The key parameters affecting the formation of $ClNO_2$ concentrations are temperature, NO_3 loss, N_2O_5 loss. Their impact on the model results is discussed below.

Fig. 6(b) shows the dependence of modelled $ClNO_2$ on the temperature and NO_2 concentrations investigated by the same model approach, for which the O_3 concentration is fixed to 30 ppbv (representing typical O_3 level of long-range transported air). In this case, the modelled $ClNO_2$ concentrations reach maximum values at temperatures of 5 °C. For these winter-like conditions, the low temperature shifts the equilibrium between NO_3 to N_2O_5 to the side of N_2O_5. In contrast, the conversion of NO_2 to $ClNO_2$ is suppressed at high temperatures (T > 15°C) as typical conditions in August and September. Temperature also plays an important role for the value of the $ClNO_2$ production efficiency due to the shift of the equilibrium between NO_3 to N_2O_5. The significantly higher $ClNO_2$ production efficiency observed in February compared to the other seasons could be largely attributed to the low temperature at that time (Fig. 6(d)).

Sensitivity tests demonstrate that decreasing the rate of the chemical loss of NO_3 to organic compounds (Fig. S11, Supporting Information) only have small impact, while the seasonal variation of chemical loss

of NO_3 peaks in summer-like conditions due to the intense biogenic emission. The higher production efficiency could be attributed to faster than assumed conversion from N_2O_5 to $ClNO_2$, which can bring modelled and measured valued into agreement. This can be either achieved by increasing the value of the N_2O_5 uptake coefficient (Fig. S12, Supporting Information) or the yield of $ClNO_2$ in the process of the heterogeneous uptake of N_2O_5 on aerosol (Fig. S13, Supporting Information).

As mentioned above, the NO_3 reactivity is assumed to be 0.004 s^{-1} to match the observations, which is comparable to the NO_3 reactivity observed at a mountainous site in south Germany with a campaign-averaged value of 0.01 s^{-1} for nighttime conditions (Liebmann et al., 2018). As shown in the sensitivity test, a higher NO_3 reactivity leads to lower modelled $ClNO_2$ concentrations. Therefore, the low NO_3 reactivity in the model could be regarded as a lower limit given the similar biogenic-influenced environments.

In this model calculation, the aerosol surface area S_a is held constant instead of using the value measured inside the chamber, which was likely impacted by the sampling system but cannot be corrected for ambient measurement (Section 2.3). Nevertheless, the measured S_a gives some confidence that the model is not using an unrealistic lower limit.

The aerosol chemical composition also plays a role in determining the production efficiency. The yield of $ClNO_2$ from N_2O_5 heterogenous reaction ($\varphi(ClNO_2)$) can be expressed by assuming that the production of $ClNO_2$ results from the competition between Cl^- and H_2O reacting with the $H_2ONO_2^+$ intermediate formed from the N_2O_5 uptake on aerosol (Bertram and Thornton, 2009;Mielke et al., 2013;McDuffie et al., 2018b).

$$\varphi(ClNO_2)_{par} = \left(1 + \frac{[H_2O]}{50[Cl^-]}\right)^{-1} \quad \text{(Eq. 8)}$$

The value of the $ClNO_2$ yield is different in the periods of the campaign showing maximum values of 0.6 to 0.8 in February (Fig. S14, Supporting Information). This is consistent with the relatively high $ClNO_2$ production efficiency derived from the integrated production rate of NO_3 (Eq.7). However, the calculated $ClNO_2$ yield decreases below 0.4 in August and September, which could be attributed to the higher aerosol liquid water content in these two periods compared to the value in other periods (Table S1). The calculated $ClNO_2$ yield is also higher for the long-range transported air masses than those for the regional one (Fig. S14, Supporting Information). The relatively high $ClNO_2$ production efficiencies found in the regional air masses, which are in contrast to their relatively low calculated $\varphi(ClNO_2)$, suggest that other factors play an important role in determining the $ClNO_2$ production such as larger-than-assumed uptake coefficient for N_2O_5 and/or aerosol surface area.

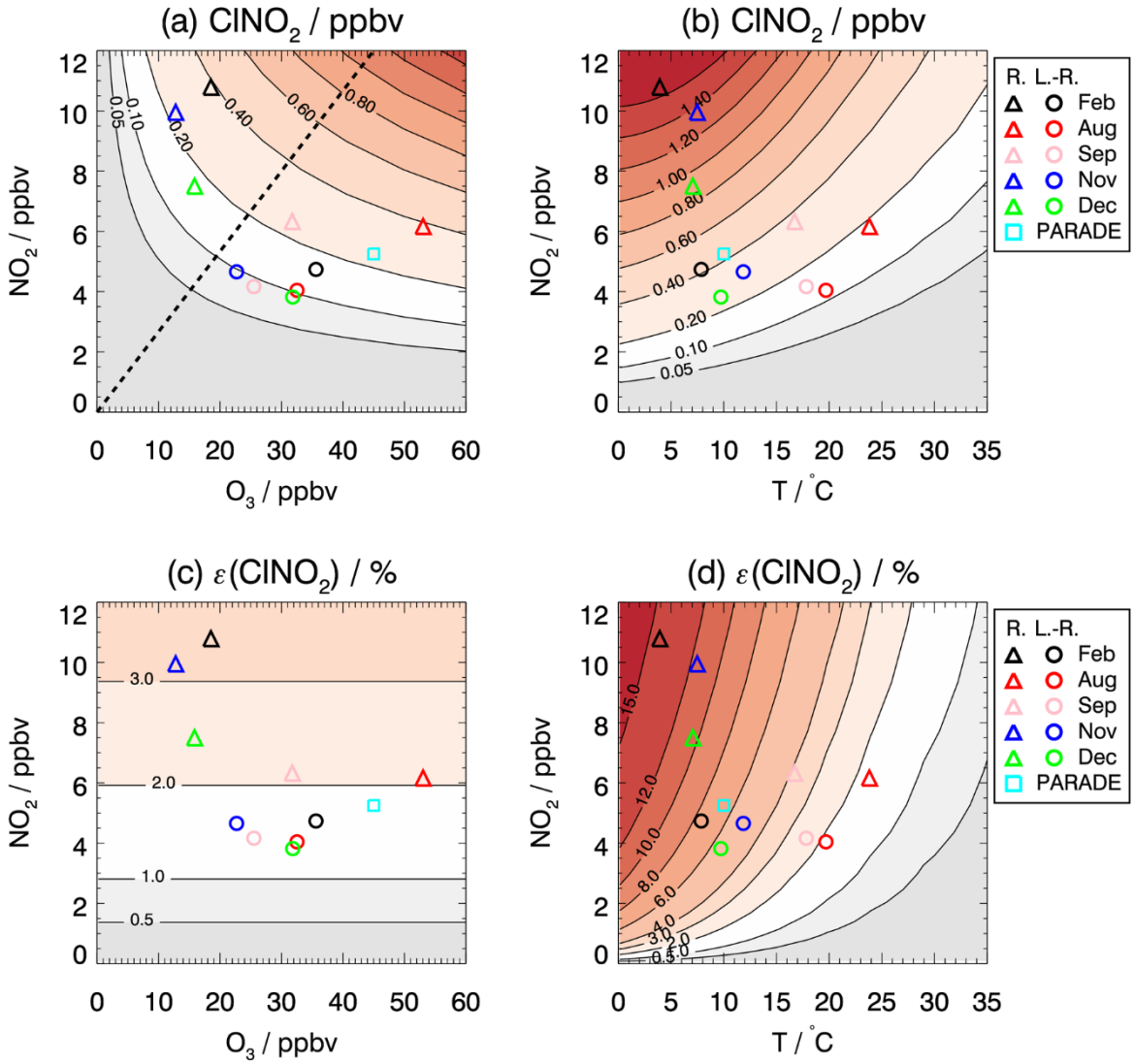

632

633 **Figure 6.** Isopleth plot of modelled (a, b) $ClNO_2$ mixing ratios that accumulate during nighttime and (c,
634 d) the $ClNO_2$ production efficiency depending on (a, c) the initial O_3 and NO_2 mixing ratios and (b, d) the
635 temperature and initial NO_2 mixing ratios. Values are taken after four hours since sunset, when maximum
636 $ClNO_2$ concentrations were observed. Symbols mark calculated $ClNO_2$ mixing ratios for average values
637 of NO_2 and O_3 mixing ratios measured in each period of the JULIAC campaign, if air masses originated
638 either from long-range (L.-R.) or regional (R.) transportation. For comparison, values are also shown for
639 measurements during the PARADE campaign in summer in Germany (Phillips et al., 2012). The dashed
640 line (panel a) separates the regimes for which $ClNO_2$ production is more sensitive to the change of O_3
641 (upper left) and NO_2 (bottom right).

642

For comparison, the observation from another field campaign conducted in a similar rural environment in Germany is marked in the isopleth diagram (Fig. 6). The PARADE campaign took place in the Taunus Observatory of the University of Frankfurt located 170 km southeast of the JULIAC measurement site (Phillips et al., 2012). The maximum observed $ClNO_2$ mixing ratio was 0.8 ppbv when the measurement site was influenced by air masses from the UK/North Sea. This value is lower than the results of the model calculations using the median NO_2 and O_3 observed in that campaign, which is consistent to the general underprediction for summer-like conditions for the JULIAC campaign, suggesting the conversion from NO_3 to $ClNO_2$ is more efficient than the model predicts in summer. The position in the isopleth diagram suggests that $ClNO_2$ formation was limited by the availability of NO_2 similar to the summer period the JULIAC campaign, the same season as the PARADE campaign (August).

4 Summary and Conclusions

Concentrations of $ClNO_2$ and other trace gases and the chemical composition of aerosols were measured during the Jülich Atmospheric Chemistry Project (JULIAC) campaign in 2019 performed at a rural site in Germany. Ambient air was sampled into the atmospheric simulation chamber SAPHIR from a height of 50 m, which, for most of the time, was uncoupled from surface layer during the night. Chamber characterization experiments demonstrated that no significant loss or production of $ClNO_2$ occurred inside the chamber for experimental conditions of the JULIAC campaign.

In all periods, $ClNO_2$ measurements showed a trend of increasing mixing ratios after sunset with maximum values were reached around midnight. This qualitative behavior is consistent with the chemical production of $ClNO_2$ and insignificant losses during the night. Photolysis was the main loss process for $ClNO_2$ on the following day. The maximum $ClNO_2$ concentration in this campaign of 1.6 ppbv was observed in September at the late-night (03:00 UTC). The analysis of the origin of air masses by calculations of back trajectories shows that mixing ratios of $ClNO_2$, NO_2 and O_3 were higher in regional air masses than in air masses that traveled a long distance.

A case study analyzing measurements in the night from 21 to 22 August 2019 shows that the stratification of layers during the night can strongly impact observed trace gas concentrations, specifically when the sampling point of the inlet system was located within a height range that was characterized by poor vertical mixing of the air. During most times of the campaign, however, the sampling point was isolated from the surface layer during the night. In this case, losses of trace gases to the surface and reactions with fresh emissions on the ground, which would typically reduce $ClNO_2$ production, were not important.

673 The $ClNO_2$ production efficiency (i.e. the number of $ClNO_2$ molecules formed per produced NO_3
674 molecule) was higher for conditions in air masses from regional areas than from long-range
675 transportation, mostly due to the higher NO_2 mixing ratios. The minimum average value of the production
676 efficiency calculated for the individual measurement periods in the JULIAC campaign was 3%,
677 experienced in December for all air masses independent from their origin. This low value can be
678 attributed to the low NO_2 mixing ratios experienced in winter. For the air masses from long-range
679 transportation, the mean $ClNO_2$ production efficiencies were in the range of 3% to 6% in the period
680 between August to November but were as high as 12% in February, consistent with the seasonality of the
681 observed $ClNO_2$ concentrations. The highest mean $ClNO_2$ production efficiency was found in February,
682 when values reached (18±9) % and NO_2 concentrations were highest in the regional air masses. High
683 $ClNO_2$ production efficiency was also found in September, when NO_2 concentrations were low,
684 suggesting that other factors including the available aerosol surface area (S_a), the variability of the N_2O_5
685 uptake coefficient, and the yield of $ClNO_2$ in the heterogeneous reaction of N_2O_5 were favoring the
686 production of $ClNO_2$.

687 With the help of a simple box model of nighttime chemistry for the NO_3-N_2O_5-$ClNO_2$ system, the
688 dependence of $ClNO_2$ concentration on the availability of O_3 and NO_2 was investigated. The purpose of
689 such simplified model is to demonstrate the general feature of ClNO2 production versus chemical
690 conditions but not to compare with observations. The model results suggest that $ClNO_2$ production was
691 more sensitive to the availability of NO_2 than that of O_3, especially the air masses from long-range
692 transportation. The seasonal variability of $ClNO_2$ is less pronounced compared to the seasonal changes of
693 NO_2 and O_3 concentrations, because changes in the NO_2 and O_3 concentrations partly compensated for
694 each other. The simple model cannot predict the seasonal changes in the observed $ClNO_2$ mixing ratios.
695 This indicates that processes other than the NO_3 production rate significantly impacted the $ClNO_2$ mixing
696 ratios. Nevertheless, this simple model approach helps to understand the general features of the
697 dependence of $ClNO_2$ concentrations on the availability of NO_2 and O_3 in the JULIAC campaign.

698

699 **Data availability**

700 The data used in this study are available on the Jülich DATA platform (https://doi.org/10.26165/JUELICH-
701 DATA/XG6YGZ).

702 **Author contributions**

AH designed JULIAC campaign and organized it together with HF and FH. ZT and RS performed the measurements of $ClNO_2$ and analyzed the data. ZT, RS, HF, and AH wrote the paper. All co-authors contributed with data and commented and discussed the manuscript and contributed to the writing of the manuscript.

Competing interests

Some authors are members of the editorial board of Atmospheric Chemistry and Physics. The authors declare that they have no conflict of interest.

Acknowledgements

The authors thank the scientific team of JULIAC campaign for logistical support, the Chemistry Workshop and Glassblower of the University of Leicester for technical support

Financial Support.

This project has been supported by the BMBF project ID-CLAR (grant no. 01DO17036) and BMBF project PRACTICE (grant no. 01LP1929A), the European Research Council (ERC) and European Commission (EC) under the European Union's Horizon 2020 research and innovation program (SARLEP grant agreement no. 681529 and Eurochamp 2020 grant agreement no. 730997).

References:

Atkinson, R., Baulch, D. L., Cox, R. A., Crowley, J. N., Hampson, R. F., Hynes, R. G., Jenkin, M. E., Rossi, M. J., and Troe, J.: Evaluated kinetic and photochemical data for atmospheric chemistry: Volume I - gas phase reactions of Ox, HOx, NOx and SOx species, Atmos. Chem. Phys., 4, 1461-1738, 10.5194/acp-4-1461-2004, 2004.

Bannan, T. J., Booth, A. M., Bacak, A., Muller, J. B. A., Leather, K. E., Le Breton, M., Jones, B., Young, D., Coe, H., Allan, J., Visser, S., Slowik, J. G., Furger, M., Prévôt, A. S. H., Lee, J., Dunmore, R. E., Hopkins, J. R., Hamilton, J. F., Lewis, A. C., Whalley, L. K., Sharp, T., Stone, D., Heard, D. E., Fleming, Z. L., Leigh, R., Shallcross, D. E., and Percival, C. J.: The first UK measurements of nitryl chloride using a chemical ionization mass spectrometer in central London in the summer of 2012, and an investigation of the role of Cl atom oxidation, J. Geophys. Res., 120, 5638-5657, 10.1002/2014JD022629, 2015.

Bertram, T. H., and Thornton, J. A.: Toward a general parameterization of N2O5 reactivity on aqueous particles: the competing effects of particle liquid water, nitrate and chloride, Atmos. Chem. Phys., 9, 8351-8363, 10.5194/acp-9-8351-2009, 2009.

734 Bohn, B., Rohrer, F., Brauers, T., and Wahner, A.: Actinometric measurements of NO2 photolysis
735 frequencies in the atmosphere simulation chamber SAPHIR, Atmos. Chem. Phys., 5, 493-503,
736 10.5194/acp-5-493-2005, 2005.

737 Brown, S. S., Dubé, W. P., Osthoff, H. D., Wolfe, D. E., Angevine, W. M., and Ravishankara, A. R.:
738 High resolution vertical distributions of NO₃ and N₂O₅
739 through the nocturnal boundary layer, Atmos. Chem. Phys., 7, 139-149, 10.5194/acp-7-139-2007,
740 2007.

741 Brown, S. S., and Stutz, J.: Nighttime radical observations and chemistry, Chem. Soc. Rev., 41, 6405-
742 6447, 10.1039/c2cs35181a, 2012.

743 Eger, P. G., Friedrich, N., Schuladen, J., Shenolikar, J., Fischer, H., Tadic, I., Harder, H., Martinez, M.,
744 Rohloff, R., Tauer, S., Drewnick, F., Fachinger, F., Brooks, J., Darbyshire, E., Sciare, J., Pikridas,
745 M., Lelieveld, J., and Crowley, J. N.: Shipborne measurements of ClNO2 in the Mediterranean
746 Sea and around the Arabian Peninsula during summer, Atmos. Chem. Phys., 19, 12121-12140,
747 10.5194/acp-19-12121-2019, 2019.

748 George, I. J., and Abbatt, J. P. D.: Heterogeneous oxidation of atmospheric aerosol particles by gas-
749 phase radicals, Nat. Chem., 2, 713, 10.1038/nchem.806, 2010.

750 Jeong, D., Seco, R., Gu, D., Lee, Y., Nault, B. A., Knote, C. J., McGee, T., Sullivan, J. T., Jimenez, J.
751 L., Campuzano-Jost, P., Blake, D. R., Sanchez, D., Guenther, A. B., Tanner, D., Huey, L. G.,
752 Long, R., Anderson, B. E., Hall, S. R., Ullmann, K., Shin, H., Herndon, S. C., Lee, Y., Kim, D.,
753 Ahn, J., and Kim, S.: Integration of airborne and ground observations of nitryl chloride in the
754 Seoul metropolitan area and the implications on regional oxidation capacity during KORUS-AQ
755 2016, Atmos. Chem. Phys., 19, 12779-12795, 10.5194/acp-19-12779-2019, 2019.

756 Kercher, J., Riedel, T., and Thornton, J.: Chlorine activation by N2O5: simultaneous, in situ detection
757 of ClNO2 and N2O5 by chemical ionization mass spectrometry, Atmos. Meas. Tech., 2, 193-204,
758 10.5194/amt-2-193-2009, 2009.

759 Le Breton, M., Hallquist, Å. M., Pathak, R. K., Simpson, D., Wang, Y., Johansson, J., Zheng, J., Yang,
760 Y., Shang, D., Wang, H., Liu, Q., Chan, C., Wang, T., Bannan, T. J., Priestley, M., Percival, C. J.,
761 Shallcross, D. E., Lu, K., Guo, S., Hu, M., and Hallquist, M.: Chlorine oxidation of VOCs at a
762 semi-rural site in Beijing: significant chlorine liberation from ClNO2 and subsequent gas- and
763 particle-phase Cl–VOC production, Atmos. Chem. Phys., 18, 13013-13030, 10.5194/acp-18-
764 13013-2018, 2018.

765 Liebmann, J. M., Muller, J. B. A., Kubistin, D., Claude, A., Holla, R., Plass-Dülmer, C., Lelieveld, J.,
766 and Crowley, J. N.: Direct measurements of NO3 reactivity in and above the boundary layer of a
767 mountaintop site: identification of reactive trace gases and comparison with OH reactivity, Atmos.
768 Chem. Phys., 18, 12045-12059, 10.5194/acp-18-12045-2018, 2018.

769 Liu, X., Qu, H., Huey, L. G., Wang, Y., Sjostedt, S., Zeng, L., Lu, K., Wu, Y., Hu, M., Shao, M., Zhu,
770 T., and Zhang, Y.: High Levels of Daytime Molecular Chlorine and Nitryl Chloride at a Rural Site
771 on the North China Plain, Environ. Sci. Technol., 51, 9588-9595, 10.1021/acs.est.7b03039, 2017.

772 Lou, S., Tan, Z., Gan, G., Chen, J., Wang, H., Gao, Y., Huang, D., Huang, C., Li, X., Song, R., Wang,
773 H., Wang, M., Wang, Q., Wu, Y., and Huang, C.: Observation based study on atmospheric

oxidation capacity in Shanghai during late-autumn: Contribution from nitryl chloride, Atmos. Environ., 271, 118902, 10.1016/j.atmosenv.2021.118902, 2022.

McDuffie, E. E., Fibiger, D. L., Dubé, W. P., Lopez-Hilfiker, F., Lee, B. H., Thornton, J. A., Shah, V., Jaeglé, L., Guo, H., Weber, R. J., Michael Reeves, J., Weinheimer, A. J., Schroder, J. C., Campuzano-Jost, P., Jimenez, J. L., Dibb, J. E., Veres, P., Ebben, C., Sparks, T. L., Wooldridge, P. J., Cohen, R. C., Hornbrook, R. S., Apel, E. C., Campos, T., Hall, S. R., Ullmann, K., and Brown, S. S.: Heterogeneous N2O5 Uptake During Winter: Aircraft Measurements During the 2015 WINTER Campaign and Critical Evaluation of Current Parameterizations, J. Geophys. Res., 123, 4345-4372, 10.1002/2018jd028336, 2018a.

McDuffie, E. E., Fibiger, D. L., Dubé, W. P., Lopez Hilfiker, F., Lee, B. H., Jaeglé, L., Guo, H., Weber, R. J., Reeves, J. M., Weinheimer, A. J., Schroder, J. C., Campuzano-Jost, P., Jimenez, J. L., Dibb, J. E., Veres, P., Ebben, C., Sparks, T. L., Wooldridge, P. J., Cohen, R. C., Campos, T., Hall, S. R., Ullmann, K., Roberts, J. M., Thornton, J. A., and Brown, S. S.: ClNO2 Yields From Aircraft Measurements During the 2015 WINTER Campaign and Critical Evaluation of the Current Parameterization, J. Geophys. Res., 123, 12,994-913,015, 10.1029/2018jd029358, 2018b.

McNamara, S. M., Kolesar, K. R., Wang, S., Kirpes, R. M., May, N. W., Gunsch, M. J., Cook, R. D., Fuentes, J. D., Hornbrook, R. S., Apel, E. C., China, S., Laskin, A., and Pratt, K. A.: Observation of Road Salt Aerosol Driving Inland Wintertime Atmospheric Chlorine Chemistry, ACS Cent. Sci., 6, 684-694, 10.1021/acscentsci.9b00994, 2020.

Mielke, L. H., Furgeson, A., and Osthoff, H. D.: Observation of ClNO2 in a mid-continental urban environment, Environ. Sci. Technol., 45, 8889-8896, 10.1021/es201955u, 2011.

Mielke, L. H., Stutz, J., Tsai, C., Hurlock, S. C., Roberts, J. M., Veres, P. R., Froyd, K. D., Hayes, P. L., Cubison, M. J., Jimenez, J. L., Washenfelder, R. A., Young, C. J., Gilman, J. B., de Gouw, J. A., Flynn, J. H., Grossberg, N., Lefer, B. L., Liu, J., Weber, R. J., and Osthoff, H. D.: Heterogeneous formation of nitryl chloride and its role as a nocturnal NOx reservoir species during CalNex-LA 2010, J. Geophys. Res., 118, 10,638-610,652, 10.1002/jgrd.50783, 2013.

Mielke, L. H., Furgeson, A., Odame-Ankrah, C. A., and Osthoff, H. D.: Ubiquity of ClNO2 in the urban boundary layer of Calgary, Alberta, Canada, Can. J. Chem., 94, 414-423, 10.1139/cjc-2015-0426, 2016.

Osthoff, H. D., Roberts, J. M., Ravishankara, A. R., Williams, E. J., Lerner, B. M., Sommariva, R., Bates, T. S., Coffman, D., Quinn, P. K., Dibb, J. E., Stark, H., Burkholder, J. B., Talukdar, R. K., Meagher, J., Fehsenfeld, F. C., and Brown, S. S.: High levels of nitryl chloride in the polluted subtropical marine boundary layer, Nat. Geosci., 1, 324-328, 10.1038/ngeo177, 2008.

Osthoff, H. D., Odame-Ankrah, C. A., Taha, Y. M., Tokarek, T. W., Schiller, C. L., Haga, D., Jones, K., and Vingarzan, R.: Low levels of nitryl chloride at ground level: nocturnal nitrogen oxides in the Lower Fraser Valley of British Columbia, Atmos. Chem. Phys., 18, 6293-6315, 10.5194/acp-18-6293-2018, 2018.

Phillips, G. J., Tang, M. J., Thieser, J., Brickwedde, B., Schuster, G., Bohn, B., Lelieveld, J., and Crowley, J. N.: Significant concentrations of nitryl chloride observed in rural continental Europe associated with the influence of sea salt chloride and anthropogenic emissions, Geophys. Res. Lett., 39, 10.1029/2012gl051912, 2012.

Priestley, M., le Breton, M., Bannan, T. J., Worrall, S. D., Bacak, A., Smedley, A. R. D., Reyes-Villegas, E., Mehra, A., Allan, J., Webb, A. R., Shallcross, D. E., Coe, H., and Percival, C. J.: Observations of organic and inorganic chlorinated compounds and their contribution to chlorine radical concentrations in an urban environment in northern Europe during the wintertime, Atmos. Chem. Phys., 18, 13481-13493, 10.5194/acp-18-13481-2018, 2018.

Riedel, T. P., Wagner, N. L., Dube, W. P., Middlebrook, A. M., Young, C. J., Ozturk, F., Bahreini, R., VandenBoer, T. C., Wolfe, D. E., Williams, E. J., Roberts, J. M., Brown, S. S., and Thornton, J. A.: Chlorine activation within urban or power plant plumes: Vertically resolved ClNO2 and Cl-2 measurements from a tall tower in a polluted continental setting, J. Geophys. Res., 118, 8702-8715, 10.1002/jgrd.50637, 2013.

Roberts, J. M., Osthoff, H. D., Brown, S. S., Ravishankara, A. R., Coffman, D., Quinn, P., and Bates, T.: Laboratory studies of products of N2O5 uptake on Cl− containing substrates, Geophys. Res. Lett., 36, 10.1029/2009gl040448, 2009.

Rohrer, F., Bohn, B., Brauers, T., Brüning, D., Johnen, F. J., Wahner, A., and Kleffmann, J.: Characterisation of the photolytic HONO-source in the atmosphere simulation chamber SAPHIR, Atmos. Chem. Phys., 5, 2189-2201, 10.5194/acp-5-2189-2005, 2005.

Simpson, W. R., Brown, S. S., Saiz-Lopez, A., Thornton, J. A., and von Glasow, R.: Tropospheric Halogen Chemistry: Sources, Cycling, and Impacts, Chem. Rev., 115, 4035-4062, 10.1021/cr5006638, 2015.

Sommariva, R., Hollis, L. D. J., Sherwen, T., Baker, A. R., Ball, S. M., Bandy, B. J., Bell, T. G., Chowdhury, M. N., Cordell, R. L., Evans, M. J., Lee, J. D., Reed, C., Reeves, C. E., Roberts, J. M., Yang, M., and Monks, P. S.: Seasonal and geographical variability of nitryl chloride and its precursors in Northern Europe, Atmos. Sci. Lett., 19, e844, 10.1002/asl.844, 2018.

Sommariva, R., Crilley, L. R., Ball, S. M., Cordell, R. L., Hollis, L. D. J., Bloss, W. J., and Monks, P. S.: Enhanced wintertime oxidation of VOCs via sustained radical sources in the urban atmosphere, Environ. Pollut., 274, 116563, 10.1016/j.envpol.2021.116563, 2021.

Stein, A. F., Draxler, R. R., Rolph, G. D., Stunder, B. J. B., Cohen, M. D., and Ngan, F.: NOAA's HYSPLIT Atmospheric Transport and Dispersion Modeling System, Bull. Am. Meteorol. Soc., 96, 2059-2077, 10.1175/bams-d-14-00110.1, 2015.

Tham, Y. J., Wang, Z., Li, Q., Yun, H., Wang, W., Wang, X., Xue, L., Lu, K., Ma, N., Bohn, B., Li, X., Kecorius, S., Größ, J., Shao, M., Wiedensohler, A., Zhang, Y., and Wang, T.: Significant concentrations of nitryl chloride sustained in the morning: investigations of the causes and impacts on ozone production in a polluted region of northern China, Atmos. Chem. Phys., 16, 14959-14977, 10.5194/acp-16-14959-2016, 2016.

Thornton, J. A., Kercher, J. P., Riedel, T. P., Wagner, N. L., Cozic, J., Holloway, J. S., Dube, W. P., Wolfe, G. M., Quinn, P. K., Middlebrook, A. M., Alexander, B., and Brown, S. S.: A large atomic chlorine source inferred from mid-continental reactive nitrogen chemistry, Nature, 464, 271-274, 10.1038/nature08905, 2010.

Wagner, N. L., Dubé, W. P., Washenfelder, R. A., Young, C. J., Pollack, I. B., Ryerson, T. B., and Brown, S. S.: Diode laser-based cavity ring-down instrument for NO₃,

N₂O₅, NO, NO₂ and O₃ from aircraft, Atmos. Meas. Tech., 4, 1227-1240, 10.5194/amt-4-1227-2011, 2011.

Wagner, N. L., Riedel, T. P., Roberts, J. M., Thornton, J. A., Angevine, W. M., Williams, E. J., Lerner, B. M., Vlasenko, A., Li, S. M., Dube, W. P., Coffman, D. J., Bon, D. M., de Gouw, J. A., Kuster, W. C., Gilman, J. B., and Brown, S. S.: The sea breeze/land breeze circulation in Los Angeles and its influence on nitryl chloride production in this region, J. Geophys. Res., 117, 10.1029/2012jd017810, 2012.

Wang, T., Tham, Y. J., Xue, L., Li, Q., Zha, Q., Wang, Z., Poon, S. C. N., Dubé, W. P., Blake, D. R., Louie, P. K. K., Luk, C. W. Y., Tsui, W., and Brown, S. S.: Observations of nitryl chloride and modeling its source and effect on ozone in the planetary boundary layer of southern China, J. Geophys. Res., 121, 2476-2489, 10.1002/2015JD024556, 2016.

Wang, X., Wang, H., Xue, L., Wang, T., Wang, L., Gu, R., Wang, W., Tham, Y. J., Wang, Z., Yang, L., Chen, J., and Wang, W.: Observations of N2O5 and ClNO2 at a polluted urban surface site in North China: High N2O5 uptake coefficients and low ClNO2 product yields, Atmos. Environ., 156, 125-134, 10.1016/j.atmosenv.2017.02.035, 2017a.

Wang, Z., Wang, W., Tham, Y. J., Li, Q., Wang, H., Wen, L., Wang, X., and Wang, T.: Fast heterogeneous N2O5 uptake and ClNO2 production in power plant and industrial plumes observed in the nocturnal residual layer over the North China Plain, Atmos. Chem. Phys., 17, 12361-12378, 10.5194/acp-17-12361-2017, 2017b.

Yan, C., Tham, Y. J., Zha, Q., Wang, X., Xue, L., Dai, J., Wang, Z., and Wang, T.: Fast heterogeneous loss of N2O5 leads to significant nighttime NOx removal and nitrate aerosol formation at a coastal background environment of southern China, Sci. Total Environ., 677, 637-647, 10.1016/j.scitotenv.2019.04.389, 2019.

Young, C. J., Washenfelder, R. A., Roberts, J. M., Mielke, L. H., Osthoff, H. D., Tsai, C., Pikelnaya, O., Stutz, J., Veres, P. R., Cochran, A. K., VandenBoer, T. C., Flynn, J., Grossberg, N., Haman, C. L., Lefer, B., Stark, H., Graus, M., de Gouw, J., Gilman, J. B., Kuster, W. C., and Brown, S. S.: Vertically resolved measurements of nighttime radical reservoirs in Los Angeles and their contribution to the urban radical budget, Environ. Sci. Technol., 46, 10965-10973, 10.1021/es302206a, 2012.

Yun, H., Wang, T., Wang, W., Tham, Y. J., Li, Q., Wang, Z., and Poon, S. C. N.: Nighttime NOx loss and ClNO2 formation in the residual layer of a polluted region: Insights from field measurements and an iterative box model, Sci. Total Environ., 622-623, 727-734, 10.1016/j.scitotenv.2017.11.352, 2018.

Zhou, W., Zhao, J., Ouyang, B., Mehra, A., Xu, W., Wang, Y., Bannan, T. J., Worrall, S. D., Priestley, M., Bacak, A., Chen, Q., Xie, C., Wang, Q., Wang, J., Du, W., Zhang, Y., Ge, X., Ye, P., Lee, J. D., Fu, P., Wang, Z., Worsnop, D., Jones, R., Percival, C. J., Coe, H., and Sun, Y.: Production of N2O5 and ClNO2 in summer in urban Beijing, China, Atmos. Chem. Phys., 18, 11581-11597, 10.5194/acp-18-11581-2018, 2018.